Lasers in Manufacturing Conference 2021

Investigations on the weld seam geometry of ultrasonic assisted laser beam welded round bars in and beside antinode position

J. Grajczak[a, *], C. Nowroth[b], J. Twiefel[b], J. Wallaschek[b], S. Nothdurft[a], J. Hermsdorf[a], V. Wesling[c], S. Kaierle[a]

[a]*Laser Zentrum Hannover e.V., Hollerithallee 8, 30419 Hannover, Germany*
[b]*institute of Dynamics and Vibration Research, Leibniz University Hannover, An der Universität 1, 30823 Garbsen, Germany*
[c]*Technische Universität Clausthal, Adolph-Roemer-Straße 2a, 38678 Clausthal-Zellerfeld, Germany*

Abstract

Laser beam welds are usually symmetric. They can form asymmetric weld seams by introducing ultrasound, which normally can be used for grain refinement and reducing segregation. The investigations comprise ultrasonic assisted laser beam welding around antinode position of a stationary ultrasonic wave.
The experiments are carried out with 2.4856 round bars, a laser beam power of 6 kW, a welding speed of 0.95 m/min and ultrasonic amplitudes of 0 µm and 4 µm. The welding positions are placed 0/7.5/15.0 mm on the right and left side of antinode position. Afterwards, specimen macrographs and micrographs of metallographic cross sections are made. As a result, the direction dependent asymmetry of the weld seams due to the position in the vibration distribution was proved. In addition, two different approaches are described to explain the fluid dynamic processes.

Keywords: laser beam welding ; ultrasound ; excitation methods ; melt pool dynamics ; nickel base alloy 2.4856

1. Introduction

Nickel alloys with an addition of about 20 % chromium have high corrosion resistance and high strength at elevated temperatures. So, they are commonly used for high-temperature applications and in corrosive environments like for fan blades in turbines or as parts in chemical plants (Zhou et al., 2018). There are several trade names for this material group like Inconel, Chronin or Nicrofer. Welding of highly alloyed nickel is as

* Corresponding author. Tel.: +49 511 2788-391; fax: +49 511 2788-100.
E-mail address: j.grajczak@lzh.de.

problematic as welding stainless steel, because segregation is likely to occur due to a high amount of alloying elements. Those can form lately solidifying phases between the primary grains, and effect hot cracking (Zhou et al., 2018). In addition, segregated alloying elements are missing in the residual material, which changes properties like corrosion resistance in the case of missing chromium (Lee and Wu, 2010).

Ultrasonic excitation of solidifying melt can be used for melt mixing (Zhou et al., 2018). Hence, it can prevent segregation and foster a finer grain structure, because dendrites break through mixing, which in turn creates more nucleation sites (Dommaschk and Hübler, 2003). A finer grain structure improves strength and ductility (Nothdurft et al., 2019). Another effect of high amplitude ultrasonic excitation is acoustic cavitation, which occurs in fluids and can be divided into gas bubble cavitation and vapour bubble cavitation. In vapour bubble cavitation, fluid turns to gas when its pressure becomes low enough. This gas bubble implodes immediately, when the pressure rises sufficiently high for condensation. In result, liquid is drawn into the generated vacuum and a pressure shock of around 1000 Pa with temperatures of about 10,000 K occurs (Wendt, 1996). Close to solid interfaces, a liquid micro jet, caused by an imploded bubble, can damage the interface. In ultrasonic assisted welding, cavitation may happen in the melt pool. For a stationary wave, cavitation is unlikely to occur in a melt pool at nodal position. Gas bubble cavitation occurs when gas is present in a liquid. When the pressure changes periodically by ultrasonic excitation the gas itself can form bigger bubbles or bubbles can grow at the surface of particles. Such big bubbles rise up by buoyancy, even if they shrink slightly when the ultrasonic pressure increases again (Wendt, 1996). Puschmann et al (Puschmann et al., 2020) investigated laser beam brazing with a brazing wire excited by stationary ultrasound and simulated the stationary ultrasound influence with a water-filled glass tube, which density and vapour pressure are similar to aluminium melt. Inserting the excited wire into the water-filled tube, cavitation bubbles appear in vibration antinode position. In addition, the bubbles move towards vibration node position and gather there. The wire temperature increases in antinode position due to internal friction, but the wire tip does not heat up because of its free oscillation (Puschmann et al., 2020).

Ultrasonic excitation also influences the melt pool dynamics due to the effect of acoustic streaming, which is an explanation for the cavitation bubble movement in (Puschmann et al., 2020). While the low density bubbles are moving towards vibration antinode position, crystalline particles in a glass melt in (Gerlach et al., 2001) and ice particles in an ice aerosol in (Bauerecker and Neidhart, 1998) are moving towards the pressure nodes of an ultrasonic field. Because of the possibility of inducing a time-dependent unidirectional flow besides an oscillating motion (Wu, 2018), the possibility of effecting asymmetrical welds is suggested. Wu (Wu, 2018) gives a mathematical overview of how a fluid flow can be generated by ultrasound and assumes that

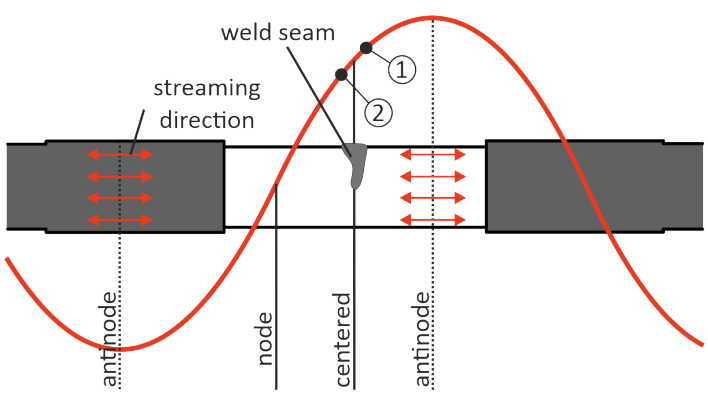

Fig. 1. Influence of wave-position on the weld seam and the difference of the vibration amplitude at the right side and the left side of the melt pool (position 1 and 2)

the flow force in a standing wave originates at the wave antinode. If the molten pool is located in this position, it is loaded equally and a symmetrical seam results. If the molten pool is located in the wave node, the same applies, because a symmetrical influence is created again due to the same distance to the left and right wave antinode, cf. Fig. 1.

If welding is carried out in an intermediate position, the distance to one wave antinode is smaller than to the other wave antinode. Wang et al (Wang et al., 2017) investigated the influence of acoustic streaming on the solidification process of an Al_2Cu alloy and describe that the force emanating from acoustic streaming depends strongly on the distance to the antinode. It leads to the assumption that the asymmetrical weld seam is a result of a force difference due to the unequal distances, which causes a material flow to one side. Völkers et al (Völkers et al., 2020) investigated the influence of 0.0/7.5/15.0/23.4 kHz sound wave superposition on laser welding of 7000 series aluminium alloy and only observed a directed change of the weld seam shape at 23.4 kHz. In result, the shape change tendency increases with increasing sound wave frequency, which equals increasing sound wave power. In the upper weld area, which can be shifted to one side by ultrasonic excitation, the melt flow is determined by Marangoni convection. It is driven by differences in surface tension and effects a melt flow from areas of low surface tension to areas of high surface tension. Depending on alloying elements and shielding gas, the surface tension can either rise or fall with rising temperature. With falling surface tension, the melt at the weld surface flows away from the hot keyhole and the melt pool is elongated in longitudinal direction (Fuhrich et al., 2001; Rai et al., 2008). In result, to change the upper weld shape, the Marangoni convection force transverse to the welding direction has to be overcome or the surface tension conditions have to be changed.

Spatter can occur if a welding process is unstable. With laser beam welding velocities below 5 m/min, it mostly originates at the keyhole edge (Weberpals and Graf, 2010). Reasons for spatter can be various and complex mechanisms in keyhole movement or melt pool dynamics, which create for example waves at the melt pool surface. Measures against spatter creation have to stabilize the welding process for example by defocussing, changing the welding velocity or changing the laser beam angle (Volpp, 2017).

Ultrasonic excitation was applied in many cases for welding steel and aluminium alloys. Zhou et al. (Zhou et al., 2018) conduct ultrasonic assisted pulsed laser welding on dissimilar welds of nickel-based Hastelloy C-276 with austenitic stainless steel 304 in lap configuration. Segregation is strongly reduced, but no grain refinement occurs.

In previous simulations (Ohrdes et al., 2021) and experiments (Grajczak et al., 2020; Nothdurft et al., 2020, 2019; Ohrdes et al., 2021) on stainless steel, aluminium alloy and nickel-base alloy, suitable parameters for the following investigations were found. Simulating ultrasonic excitation in antinode position on a liquid pool shows, that the liquid is pushed up at the solid wall sides and can be ejected at very high excitation levels. In result, a V-shaped weld seam collapse forms, which is experimentally proved (Ohrdes et al., 2021). Furthermore, asymmetric welds are created in centred and antinode position at ultrasonic amplitudes above 2 µm, but not in node position (Grajczak et al., 2020). In the following study the formation mechanism of weld asymmetry in ultrasonic assisted laser beam welding of a nickel-base alloy, see Table 1, is investigated to provide a deeper understanding of ultrasound interaction with the weld pool. Resulting pore and crack formation was discussed in (Grajczak et al., 2020). The weld seams will be evaluated by visual inspection and metallographic cross sections.

Table 1. Chemical composition of 2.4856 nickel-base alloy (VDM Metals, 2018)

Element in wt.-%	Ni	Cr	Fe	C	Mn	Si	Co	Al	Ti	P	S	Mo	Nb + Ta
Minimum	58	21										8.00	3.20
Maximum	71	23	5.00	0.03	0.50	0.40	1.00	0.40	0.40	0.01	0.01	10.00	3.80

2. Experimental setup

2.1. Laser beam welding setup

For laser beam welding tests, a diode-pumped solid state disk laser beam source (TruDisk 16002, Trumpf, Ditzingen, Germany) with specifications according to Table 2 was used.

Table 2. Laser beam welding system specifications

Model	Trumpf TruDisk 16002
Wavelength in nm	1030
Optical fiber diameter in µm	200
Collimation length in mm	150
Focal length in mm	300
Focal spot diameter in µm	400

The laser processing head is held in a constant position by a robot system (KR 60 HA, Kuka AG, Augsburg, Germany) and the welding speed is provided by rotating the specimen, see Fig. 2. The complete setup is described detailed in (Ohrdes et al., 2021). Only adapters and specimens have been changed.

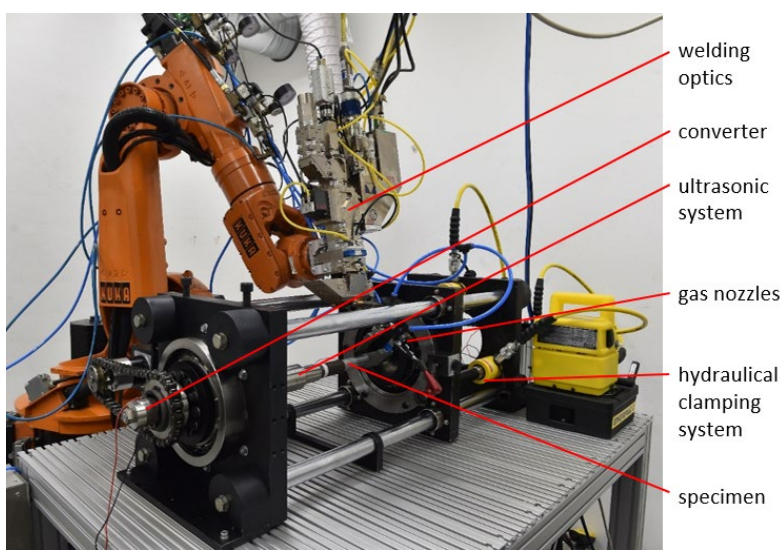

Fig. 2. Experimental setup for ultrasonic assisted laser beam welding

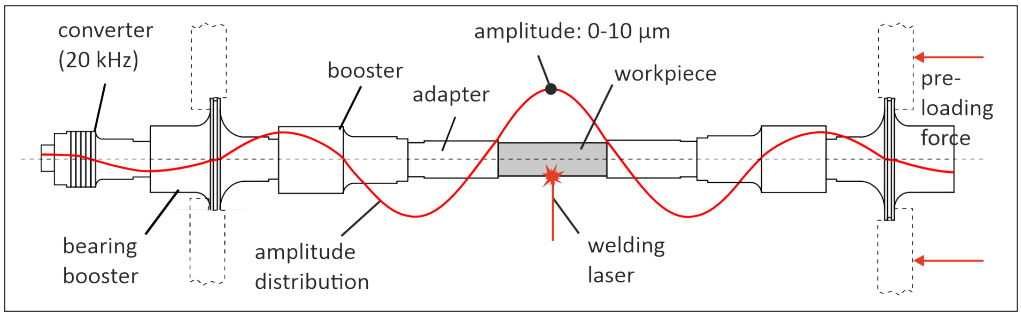

Fig. 3. Ultrasonic laser beam welding system for round bars (grey) with the vibration distribution (red)

2.2. Ultrasonic system

The specimens are part of the ultrasonic system. They are excited to resonant longitudinal oscillations in the ultrasonic range during the welding process. For this purpose, the specimens are pre-stressed in the ultrasonic system between two adapters according to Fig. 3. Besides the specimens, the system consists of adapters as well as boosters and bearing boosters both amplifying the vibration amplitude of the ultrasonic transducer up to the joining area. The vibration amplitude is adjusted in the antinode (closest one to the weld) between 0 µm and 10 µm, depending on the current amplitude set. Hence, at resonance the current amplitude is proportional to the vibration amplitude. The ultrasonic transducer (built by IDS, Institute of Dynamics and Vibration Research, Garbsen, Germany) is driven in the systems' resonance frequency (7. longitudinal mode) at approximately 20 kHz. The phase control between current and voltage of the transducer guaranties the stable operation at resonance as well as the control of the current amplitude keeps the vibration amplitude, at the closest antinode to the weld, steady. Both is carried out utilizing the control unit DPC 500/100 (Ille and Twiefel, 2015). The joint can be placed at any point of the amplitude distribution with different adapters. The system is preloaded hydraulically with preloading force high enough to prevent the components from clattering during the excited longitudinal vibration. It is selected to be 120 kN, based on a specimen diameter of 30 mm.

3. Experimental procedure

Round bars with a diameter of 30 mm and length of 65 mm made of nickel alloy 2.4856 are used as specimens for all bead on plate welds. For welding, the processing head is angled by 20°. The laser focus point is adjusted to be 4 mm in the sample and 6 mm backwards over the specimen's surface from the angular point. This laser spot orientation avoids the formation of melt drops on the specimen's surface resulting from the weight of the melt while rotating the round bars. A laser beam power of 6 kW, a welding speed of 0.95 m/min and an ultrasonic amplitude of 4 µm are used. The focal lens is protected by a cross jet while two flat nozzles provide argon as shielding gas with a pressure of 6 bar and a flow rate of 60 l/min at an angle of 45°. The flat nozzles are positioned with 50 mm distance to each other and to the specimen. The nozzles are aiming at the specimen bottom and above the specimen. The general parameters are determined by previous experiments (Grajczak et al., 2020; Nothdurft et al., 2020, 2019). According to the test plan in Table 3 three specimens are welded in different positions left and right of the ultrasound antinode position and ten specimens are welded for reference in antinode position.

Table 3: Test plan for ultrasound assisted laser beam welding of nickel-base alloy round bars

weld position in relation to antinode position in mm	−15.0	−7.5	0.0	+7.5	+15
number of specimens	3	3	10	3	3

The weld positions are determined to be ±7.5 mm and ±15.0 mm due to the stationary ultrasonic wavelength of 240 mm and the weld width of about 5 mm.

Metallographic cross sections of each specimen are prepared. The etching is conducted with CSMX-4 etchant, consisting of 100 ml H_2O, 50 ml HCl and 5 g Ferric Chloride III until the microstructure is revealed. The top and bottom weld width and weld depth are identified and evaluated.

4. Experimental results

4.1. Weld appearance

The outer weld seam appearance shows different weld pool responses to different welding positions, see Fig. 4.

All weld seams show sagging in the centre of the seam, reinforcement at the edges and directed spatters. Going from left of the antinode position to the right, the spatter is always directed away from the antinode position. The farer away from this position, the more spatters occur, but in antinode position itself, spatters

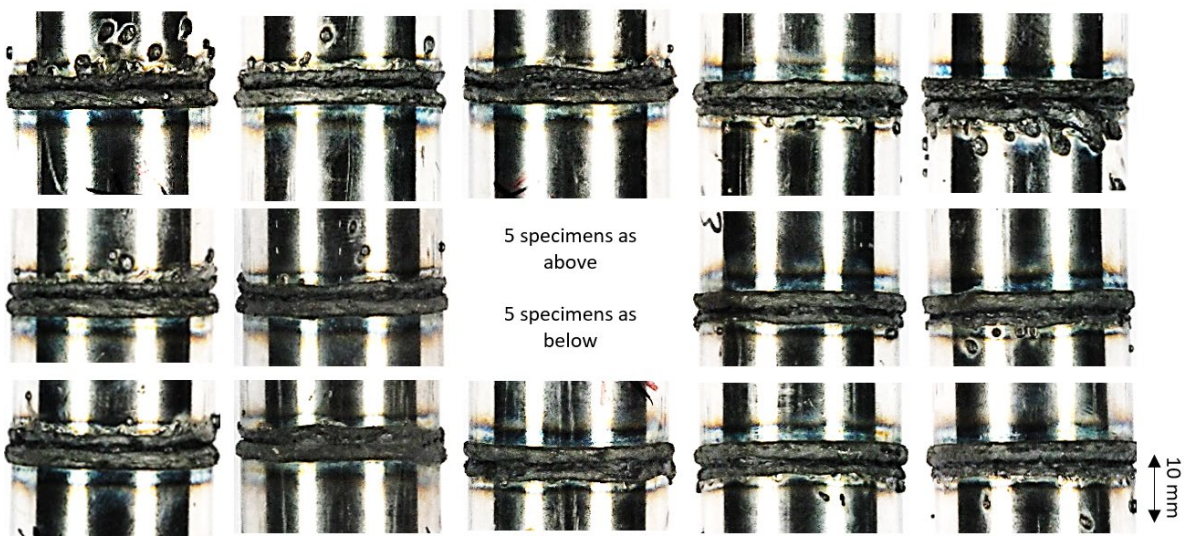

Fig. 4. Visual weld seam inspection, depicted side opposite to welding start/end point

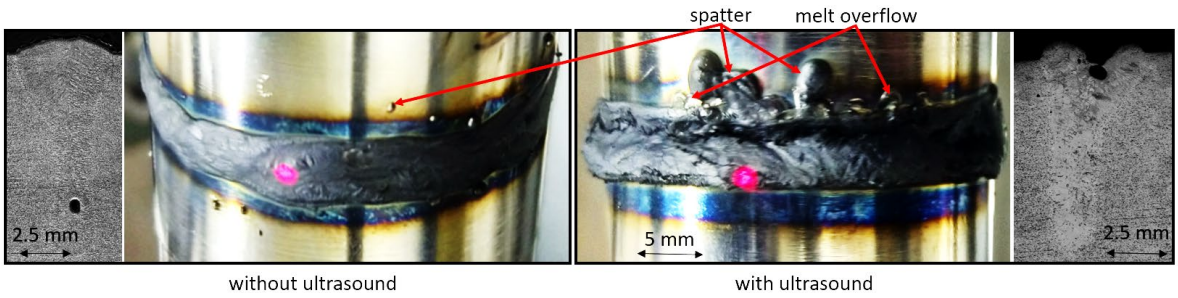

Fig. 5. Comparison of pilot laser position on weld seam with and without ultrasonic assistance including corresponding micrographs of metallographic cross sections

also occur and can be directed to the one or to the other side. In result, antinode position is adjusted correctly, but there must be influences, which prevent symmetrical weld seams or favour the ejection of melt. The passing ultrasound is very sensitive to this influences and seems to undergo a significant change from symmetrical wave distribution to asymmetrical.

After welding in antinode position with an ultrasonic amplitude of 4 µm, the pilot laser points at the weld edge in contrast to common welds, where it points at the weld middle, see Fig. 5. The uncommon pilot laser position indicates the inner weld conditions, which are revealed by metallographic cross sections. The laser beam creates a keyhole, which penetrates the specimen rectangular to its surface, but the broad upper weld area shifts towards one side due to ultrasonic excitation. In comparison to the outer appearance and pilot laser position, cf. Fig. 4 and Fig. 5, the upper welding area is shifted away from antinode position. Like in Fig. 4, the shift in antinode position can be directed to the one or to the other side, which indicates a very sensitive effect of passing ultrasound. The weld geometry is measured according to Fig. 6. The measurements left and right of the antinode position are combined because of symmetrical behaviour. The top welding width is the same for antinode position and 7.5 mm beside it, but increases slightly for a distance of 15.0 mm from antinode position. The bottom welding width increases slightly with increasing distance. The welding depth decreases by over 10 % with increasing distance. A characteristic groove forms and the spatter formation increases with increasing distance from antinode position due to increasing acoustic streaming force or other effects. A second reason for spatter formation by ultrasonic excitation is a high ultrasonic amplitude because of an upward melt movement by strongly vibrating weld interfaces, cf. (Ohrdes et al., 2021). With further increase of amplitude, the keyhole bottom can be closed, cf. (Nothdurft et al., 2020). For low ultrasonic

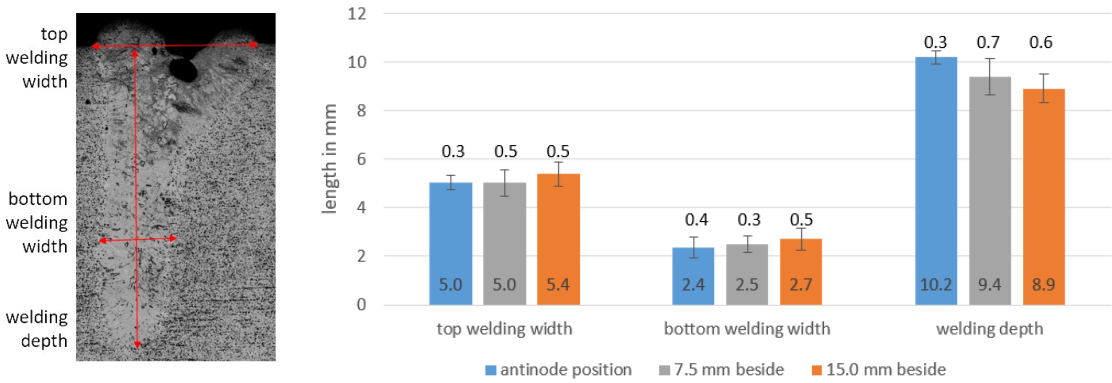

Fig. 6. Measurement of weld geometry, left: measurement example, right: measurement results including standard deviation

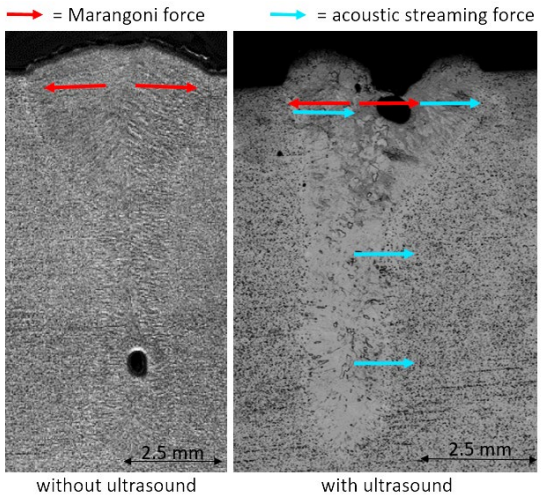

Fig. 7. Effect of Marangoni and acoustic streaming forces, cross sections

amplitudes the welds do not become asymmetric, cf. (Grajczak et al., 2020), but a groove is formed as well. For such low amplitudes, the influences of the prevailing effects are too slight.

5. Discussion

In a first approach, the acoustic streaming could lead to the observations made in chapter 4. The acoustic streaming force possibly overcomes the Marangoni convection force on one side of the weld, see Fig. 7. On its other side, the two forces superimpose and the melt flow speed is increased. In result, two types of melt ejection can be observed. First, melt overflow appears, where melt flows over the weld seam edge because the acoustic streaming force directs most melt flow into one direction. Second, small drops of spatter can be observed without ultrasonic excitation and big drops can be observed with ultrasonic excitation because the keyhole is disturbed by a cross flow of melt.

As already mentioned, the ejection of the melt could be forced due to acoustic streaming. The melt flowing away from the vibration antinode would also entrain gas bubbles, resulting in less significant pore formation. Another possible reason for the seam shift and the one-sided ejection of melt may be due to the amplitude distribution. The amplitude decreases steadily with increasing distance from the wave antinode. Since the melt pool has a certain width, the edge closer to the wave antinode (position 1) oscillates with a slightly higher amplitude than the edge further away (position 2) by the width of the melt pool, see Fig 8. The walls are vibrating with the circular frequency of $\omega = 2\pi f$, where f is the vibration frequency of around 20 kHz. A1 and

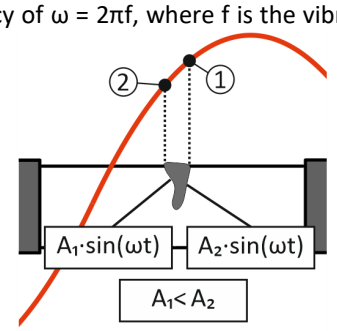

Fig. 8. Assumed amplitude difference of the melt pool edges

A2 are the vibration amplitudes the left and the right edge of the melt pool are vibrating with.The change in amplitude per millimetre is relatively small near the antinode position. However, it increases with further distance. Due to that, the difference between the two vibration amplitudes of the edges of the melt pool becomes greater. The increasing difference also makes the ejection of melt more likely, wich results in the strong ejection of melt with a position far away of the antinode. This would also explain the low, but in its direction alternating ejection of melt. In simulations for the design of the mechanical system, it was observed that the position of the vibration nodes changes slightly with the value of the preloading force. In the experiments, care is taken to set the preloading force to a constant value, but minor deviations cannot be ruled out here either. If the position of the vibration nodes and thus also the position of the vibration antinodes changes, the described case occurs that the edges of the melt pool do not have the same vibration amplitude. Since the effect close to the antinode is very small, the resulting weld seams shown above are obtained.

6. Conclusions

Following aspects about the formation of asymmetrical welds by ultrasonic excitation with a stationary wave were revealed:

- Marangoni force is superimposed by a cross flow of melt due to acoustic streaming force or a force resulting from an amplitude difference between the weld edges
- Asymmetrical welds are shallower and broader than symmetrical welds
- Small differences of clamping force result in small differences of antinode position
- Asymmetry increases with increasing distance from antinode position

The cross flow of melt influences the keyhole stability and the formation of gas porosity. On the one hand, the keyhole could be destabilized. On the other hand, pores could be removed by an increased speed of melt flow from the weld bottom to its top. But in (Grajczak et al., 2020) it was already shown that welding in a position between antinode and node results in increased porosity. In result, the formation of asymmetrical welds should be avoided by considering constant clamping forces and using suitably low ultrasonic amplitudes.

7. Outlook

The assumption that the melt pool edges oscillating with different amplitudes could lead to the ejection of melt from the melt pool will be verified in the future by means of simulations. The simplified model used previously (Ohrdes et al., 2021) can probably be adapted in the process. Other influences can also be taken into account. For example, not only the amplitude difference of the two edges of the melt pool can have an influence, but also the phase difference. This kind of simulations will be carried out in future investigations.

Acknowledgements

The authors would like to thank the German Research Foundation (DFG) for the financial and organisational support of this project. Funded by the Deutsche Forschungsgemeinschaft (DFG, German Research Foundation) - CRC 1153, subproject A3 – 252662854.

References

Bauerecker, S., Neidhart, B., 1998. Formation and growth of ice particles in stationary ultrasonic fields. The Journal of Chemical Physics 109, 3709–3712. https://doi.org/10.1063/1.476971

Dommaschk, C., Hübler, J., 2003. Auswirkungen einer Vibrationsbehandlung auf das Erstarrungs- und Speisungsverhalten von Gußwerkstoffen. Gießerei-Praxis 505–512.

Fuhrich, T., Berger, P., Hugel, H., 2001. Marangoni effect in laser deep penetration welding of steel. JOURNAL OF LASER APPLICATIONS 13, 178–186.

Gerlach, S., Rüssel, C., Avramov, I., 2001. Structurization of a partially crystalline melt by a stationary ultrasonic wave. Glass Science and Technology 74, 270–275.

Grajczak, J., Nowroth, C., Nothdurft, S., Hermsdorf, J., Twiefel, J., Wallaschek, J., Kaierle, S., 2020. Influence of Ultrasound on Pore and Crack Formation in Laser Beam Welding of Nickel-Base Alloy Round Bars. Metals 10, 1299. https://doi.org/10.3390/met10101299

Ille, I., Twiefel, J., 2015. Model-based Feedback Control of an Ultrasonic Transducer for Ultrasonic Assisted Turning Using a Novel Digital Controller. Physics procedia 70, 63–67.

Lee, H.T., Wu, J.L., 2010. Intergranular corrosion resistance of nickel-based alloy 690 weldments. Corrosion Science 52, 1545–1550. https://doi.org/10.1016/j.corsci.2010.01.030

Nothdurft, S., Ohrdes, H., Twiefel, J., Wallaschek, J., Hermsdorf, J., Overmeyer, L., Kaierle, S., 2020. Investigations on the effect of different ultrasonic amplitudes and positions in the vibration distribution on the microstructure of laser beam welded stainless steel, in: Kaierle, S., Heinemann, S.W. (Eds.), High-Power Laser Materials Processing: Applications, Diagnostics, and Systems IX, Proc. SPIE. SPIE, San Francisco, United States, p. 23. https://doi.org/10.1117/12.2566035

Nothdurft, S., Ohrdes, H., Twiefel, J., Wallaschek, J., Mildebrath, M., Maier, H.J., Hassel, T., Overmeyer, L., Kaierle, S., 2019. Influence of ultrasonic amplitude and position in the vibration distribution on the microstructure of a laser beam welded aluminum alloy. Journal of Laser Applications 31, 022402. https://doi.org/10.2351/1.5096100

Ohrdes, H., Nothdurft, S., Nowroth, C., Grajczak, J., Twiefel, J., Hermsdorf, J., Kaierle, S., Wallaschek, J., 2021. Influence of the ultrasonic vibration amplitude on the melt pool dynamics and the weld shape of laser beam welded EN AW-6082 utilizing a new excitation system for laser beam welding. Prod. Eng. Res. Devel. 15, 151–160. https://doi.org/10.1007/s11740-020-01008-0

Puschmann, M., Colditz, A., Krause, A., 2020. Steigerung der Prozesseffizienz beim Laserstrahlfügen hochfester Aluminiumlegierungen durch prozessintegrierten Einsatz von Ultraschallschwingungen. Schweißen und Schneiden 11, 710–714.

Rai, R., Kelly, S.M., Martukanitz, R.P., Debroy, T., 2008. A convective heat-transfer model for partial and full penetration keyhole mode laser welding of a structural steel. Metallurgical and Materials Transactions A, Physical Metallurgy and Materials Science 39A, 98–112. https://doi.org/10.1007/s11661-007-9400-6

Völkers, S., Scharifi, E., Sajjadifar, S.V., Böhm, S., Weidig, U., Niendorf, T., 2020. On the influence of in situ sound wave superposition on the microstructure of laser welded 7000 aluminum alloys. Journal of Advanced Joining Processes 1, 100013. https://doi.org/10.1016/j.jajp.2020.100013

Volpp, J., 2017. Dynamik und Stabilität der Dampfkapillare beim Laserstrahltiefschweißen. Dissertation, Universität Bremen.

Wang, G., Croaker, P., Dargusch, M., McGuckin, D., StJohn, D., 2017. Simulation of convective flow and thermal conditions during ultrasonic treatment of an Al-2Cu alloy. Computational materials science 134, 116–125.

Weberpals, J.-P., Graf, T., 2010. Nutzen und Grenzen guter Fokussierbarkeit beim Laserschweißen (doctoralThesis). Laser in der Materialbearbeitung - Forschungsberichte des IFSW. Universität Stuttgart, München.

Wendt, J.C., 1996. Merkblatt DVS 1004-1: Heißrissprüfverfahren Grundlagen.

Wu, J., 2018. Acoustic Streaming and Its Applications. Fluids 3, 108. https://doi.org/10.3390/fluids3040108

Zhou, S., Ma, G., Dongjiang, W., Chai, D., Lei, M., 2018. Ultrasonic vibration assisted laser welding of nickel-based alloy and Austenite stainless steel. Journal of Manufacturing Processes 31, 759–767. https://doi.org/10.1016/j.jmapro.2017.12.023